
Research Articles: Development/Plasticity/Repair

Aggrecan directs extracellular matrix mediated neuronal plasticity

D. Rowlands², K.K. Lensjø¹, T. Dinh⁴, S. Yang², M. R. Andrews³, T. Hafting^{1,4}, M. Fyhn¹, J.W. Fawcett² and G. Dick¹

¹Department of Biosciences, University of Oslo, PO Box 1066, 0316 Oslo, Norway.

²John van Geest Centre for Brain Repair, University of Cambridge, Robinson Way, Cambridge CB2 0PY, UK.

³Biological Sciences, University of Southampton, Southampton SO17 1BJ, UK.

⁴Institute of Basic Medical Sciences, University of Oslo, P.O box 1110, 0317 Oslo, Norway.

DOI: 10.1523/JNEUROSCI.1122-18.2018

Received: 4 May 2018

Revised: 31 August 2018

Accepted: 20 September 2018

Published: 3 October 2018

Author contributions: D.R., K.K.L., T.D., S.Y., M.R.A., T.H., M.F., J.W.F., and G.D. designed research; D.R., K.K.L., T.D., S.Y., M.R.A., T.H., M.F., and G.D. performed research; D.R., K.K.L., T.D., S.Y., T.H., and M.F. analyzed data; D.R., K.K.L., M.R.A., T.H., M.F., J.W.F., and G.D. wrote the first draft of the paper; D.R., K.K.L., M.F., and G.D. wrote the paper; K.K.L., T.H., M.F., J.W.F., and G.D. edited the paper; M.R.A., J.W.F., and G.D. contributed unpublished reagents/analytic tools.

Conflict of Interest: The authors declare no competing financial interests.

We want to thank Dr. Connor Quinn for assistance with image analysis, Tove Klungervik and Bård Enger Mathisen for assistance with genotyping, and Rune A. Lanton for technical assistance for imaging of optical intrinsic signals.; This work was funded by Alzheimer's Research UK (grant nr. ARUK-RF2016A-1), Christopher and Dana Reeve Foundation, the Research Council of Norway (grant nr. 143543, 143730 and 549217 to MF and 231248 to TH) and the University of Oslo.

Corresponding author: Gunnar Dick, e-mail: gunnar.dick@mn.uio.no

Cite as: J. Neurosci ; 10.1523/JNEUROSCI.1122-18.2018

Alerts: Sign up at www.jneurosci.org/cgi/alerts to receive customized email alerts when the fully formatted version of this article is published.

Aggrecan directs extracellular matrix mediated neuronal plasticity

Authors: D. Rowlands^{2†}, K.K. Lensjø^{1†}, T. Dinh⁴, S. Yang², M. R. Andrews³, T. Hafting^{1,4}, M. Fyhn¹,
J.W. Fawcett², G. Dick¹

[†]These authors contributed equally to the work

Affiliations:

¹Department of Biosciences, University of Oslo, PO Box 1066, 0316 Oslo, Norway.

²John van Geest Centre for Brain Repair, University of Cambridge, Robinson Way, Cambridge CB2 0PY, UK.

³Biological Sciences, University of Southampton, Southampton SO17 1BJ, UK.

⁴Institute of Basic Medical Sciences, University of Oslo, P.O box 1110, 0317 Oslo, Norway.

Corresponding author: Gunnar Dick, e-mail: gunnar.dick@mn.uio.no

Figures: 5 Tables: 6

Words in Abstract: 134 Words in Introduction: 280 Words in Discussion: 985

Acknowledgements:

We want to thank Dr. Connor Quinn for assistance with image analysis, Tove Klungervik and Bård Enger Mathisen for assistance with genotyping, and Rune A. Lanton for technical assistance for imaging of optical intrinsic signals.

This work was funded by Alzheimer's Research UK (grant nr. ARUK-RF2016A-1), Christopher and Dana Reeve Foundation, the Research Council of Norway (grant nr. 143543, 143730 and 549217 to MF and 231248 to TH) and the University of Oslo.

ABSTRACT: In the adult brain, the extracellular matrix (ECM) influences recovery after injury, susceptibility to mental disorders, and is in general a strong regulator of neuronal plasticity. The proteoglycan aggrecan is a core component of the condensed ECM structures termed perineuronal nets (PNNs), and the specific role of PNNs on neural plasticity remains elusive. Here, we genetically targeted the *Acan* gene encoding for aggrecan utilizing a novel animal model. This allowed for conditional and targeted loss of aggrecan *in vivo*, which ablated the PNN structure and caused a shift in the population of parvalbumin expressing inhibitory interneurons towards a high plasticity state. Selective deletion of the *Acan* gene in the visual cortex of male adult mice reinstated juvenile ocular dominance plasticity, which was mechanistically identical to critical period plasticity. Brain-wide targeting improved object recognition memory.

SIGNIFICANCE STATEMENT: The study provides the first direct evidence of aggrecan as the main functional constituent and orchestrator of PNNs, and that loss of PNNs by aggrecan removal induces a permanent state of critical period-like plasticity. Loss of aggrecan ablates the PNN structure, resulting in invoked juvenile plasticity in the visual cortex and enhanced object recognition memory.

INTRODUCTION

The capability of the brain to adapt and change alters during the lifespan, decreasing with age. This limited adult brain plasticity is advantageous to stabilize functional neuronal circuits but limits recovery of function after injury. In juvenile animals, immature cortical circuits are particularly malleable at certain stages of development termed critical periods (CPs) when adequate sensory stimuli are necessary to refine cortical circuits into functional units. Closure of the CPs and concomitant loss of juvenile plasticity coincide with maturation of inhibitory circuits (Hensch, 2004) and condensation of extracellular matrix around subtypes of neurons. These perineuronal nets (PNNs) are enriched in chondroitin sulfate proteoglycans (CSPGs) and associated matrix molecules (Hartig et al., 1994; Deepa et al., 2006). Remarkably, enzymatically degrading the CS glycosaminoglycan (GAG) component (Pizzorusso et al., 2002) or ablating the cross-linking cartilage link protein 1 (Crtl1) (Carulli et al., 2010) restores juvenile plasticity in the adult animal and affects memory and learning, as revealed by behavioral tasks such as fear memory extinction (Gogolla et al., 2009) and spontaneous object recognition (Romberg et al., 2013). However, the identity of the CSPG responsible for these effects has not been determined. Here we investigate the role of the CSPG aggrecan, a major constituent of PNNs, encoded by *Acan* (Matthews et

al., 2002). Aggrecan in PNN formation has only been studied *in vitro* (Giamanco et al., 2010; Kwok et al., 2010), as mutation in the *Acan* gene results in embryonic lethality due to the lack of cartilage in the trachea and other critical structures (Rittenhouse et al., 1978). In this study we developed a conditionally gene-targeted *Acan* mouse model to address aggrecan's role in PNN formation, plasticity, and memory function in the brain.

MATERIALS AND METHODS

Animal housing and ethics

All animal work was carried out in accordance with national law and regulation, in Cambridge in accordance with the UK Animals Scientific Procedures Act (1986) and in Oslo by the approval of the Norwegian Animal Research Committee. Animals used in this study were housed in standard housing conditions with a 12 hour light/dark cycle. Animals were housed in groups of 2-5 per cage, with the exception of one individual. Animals were fed and watered *ad libitum*.

Generation of Acan-loxP and breeding strategy

Two JM8A3.N1 embryonic stem (ES) cell lines of agouti C57BL6/N origin (Pettitt et al., 2009); #HFP0602_5_G11 and #HFP0602_5_F12, carrying the targeted *Acan* gene were purchased from the European Mouse Mutant Cell Repository (EuMMCR). The two ES cell lines are clones containing the same transgenic cassette surrounding exon 4 of the mouse *Acan* gene (Fig. 1a) a general “knock-out first” design used by the EUCOMM project, termed transgenic allele *tm1a* (Skarnes et al., 2011). Genomic DNA from the ES cell lines was analyzed by southern blotting to confirm correct genetic targeting. ES cells were plated and prepared according to the supplier's guidelines before microinjection into 50 blastocysts of albino C57BL/6J tyr^{-/-} origin and subsequent transfer to 3 pseudo pregnant females per line. The chimeric offspring, hybrid F₁ generation, was selected by appearance of coat color spots originating from transgenic cells. The F₁ animals were then crossed with albino C57BL/6J tyr^{-/-}, and transmission of genotype into G₁ generation was detected by coat color and verified by PCR genotype analysis using GT3 and WT primers (Table 1) confirming the heterozygote *tm1a* transgenic animal. The *tm1a* allele is not viable in a homozygous state, as the transgenic cassette interferes with *Acan* expression. The mouse was further crossed with the ROSA26::FLPe strain expressing FLP-*FRT* recombinase removing the majority of the transgenic cassette leading to offspring carrying the Cre-*lox* conditional knock-out allele *tm1c* (Fig. 1a), designated as the conditional knock out of *Acan*; B6(Cg)-

87 ACAN^{tm1c(EUCOMM)Hmgv>/Jwfa}, hereafter referred to as Acan-loxP. PCR genotype analysis using primer pairs
 88 FLP, tmc1, and GT5, confirmed presence of FLP recombinase and presence of *tm1c*. The *tm1c* allele is
 89 viable as a homozygote. Conditional knock-out of Acan is achieved by removing exon 4 of the *Acan* gene
 90 by Cre-lox recombination resulting in the *tm1d* allele (Fig. 1a). Loss of exon 4 induces a shift in the
 91 reading frame, and thereby prevents protein translation.

92 Brain-wide and developmental Cre-lox recombination by Nestin-CRE

93 To achieve brain-wide knock-out of *Acan*, Acan-loxP^{+/+} was crossed with Nestin-CRE (CreNes), where
 94 Cre recombinase is expressed under the control of the promoter and the nervous system-specific enhancer
 95 present in the second intron of the rat Nes gene (Tronche et al., 1999). The offspring of Acan-loxP^{+/+}
 96 CreNes mice were then back crossed for one at least one generation. The offspring of this cross; WT
 97 littermates, Acan-loxP^{+/+}, Acan-loxP^{+/+} Cre, and Acan-loxP^{+/+} Cre, were used for histological analysis and
 98 behavioral testing. Again, PCR genotype analysis was conducted using WT, GT3, GT3WT and CRE
 99 primer pairs (Table 1). All of the resulting offspring had a normal phenotype and body size (data not
 100 shown). Juvenile animals explored and developed normally and were able to rear and feed themselves
 101 (experimenter observations). All genotypes were established using PCR on genomic DNA extracted from
 102 an ear punch.

103

104

105 **Table 1: Primers used for genotyping**

106

Primer Set	Forward	Reverse	Annealing temp. (cycles)	Expected band size
CRE	5'-GCAGAACCTGAAGA TGTTTCGCGAT-3'	5'-AGGTATCTCTGACCAG AGTCATCC-3'	62°C (34 cycles)	733bp
FLP	5'-GTCCACTCCCAGGT CCAACTGCAGCCCA AG-3'	5'-CGCTAAAGAAGTATAT GTGCCTACTAACGC-3'	64°C (35 cycles)	725bp
Tm1c	5'-AAGGCGCATAACGA	5'-ACTGATGGCGAGCTCA	58°C (34 cycles)	1055bp

	TACCAC-3'	GACC-3'		
GT3	5'- GAGGGCATAACAGTC CACCAT-3'	5'- GTGGTATCGTTATGCG CCTT-3'	60°C (30 cycles)	613bp
GT3 WT	5'- GAGGGCATAACAGTC CACCAT-3'	5'- CCATCATCAGGCATTC TCCTT-3'	61°C (30 cycles)	613bp
GT5	5'- AAGGCGCATAACGA TACCAC-3'	5'- CCGCCTACTGCGACTA TAGAGA-3'	58°C (30 cycles)	7092bp (pre FLP cross) 218bp (post FLP cross)

Local and acute Cre-lox recombination by virus and retrograde tracer injection

AAV9.hSyn.HI.eGFP-Cre.WPRE.SV40 (Catalog number AV-9-PV1848) was purchased from University of Pennsylvania Vector Core, and stored at -80°C. Prior to surgery, aliquots were thawed on ice and diluted in filtered 1X PBS to a concentration of 10¹³ GC/mL. Adult mice (3-4 months old) of either Acan-loxP^{+/+} or Acan-loxP^{+/-} genotype were anesthetized with isoflurane mixed with air (5% induction, 1.0-1.8% maintenance) using a Somnosuit vaporizer (Kent Scientific, TX, USA) and a custom made mask, and placed on a controllable heating pad in a stereotaxic frame. They were injected subcutaneously with buprenorphine (0.04mg/kg) and carprofen (5 mg/kg), and bupivacaine (13 mg/kg) locally. The scalp was shaved and cleaned with 70% ethanol and chlorhexidine, and a small incision made in the skin. A craniotomy (1-1.5 mm diameter) was performed above the binocular zone of primary visual cortex using a hand-held dental drill. The virus solution was loaded into a glass pipette (opening diameter approximately 15 µm) and mounted in a Nanoject 3 micro injector (Drummond Scientific, PA, USA). A total of 500 nL was injected in a stepwise manner over 10 minutes, and the pipette left in the tissue for 10 minutes before retraction (injection coordinates relative to lambda were AP 0.0 mm, ML 3.0 mm, DV 0.5 mm). The wound was rinsed repeatedly with sterile 0.9% NaCl, and closed by suture. The animals were observed for at least one hour before they were placed back in the colony. Animals were monitored closely for a week following surgery, and given subcutaneous injections of buprenorphine and carprofen for the first three days after surgery. For retrograde tracing between V1 and the dorsal part of the lateral geniculate nucleus, Cholera toxin subunit B conjugated to AlexaFluor 488/594 was purchased from Life Technologies (CA, USA) and a 1% solution made by reconstitution in 1x PBS. Surgical procedures were as described above. The tracer injections were intentionally targeted to a more medial part of V1 to

prevent leakage into the neighboring V2L region. A total of 200nL was injected for each of the tracers at AP 0.0 mm, ML 2.7.0±0.1 mm DV 0.5mm, the injections of each conjugate separated by 0.2 mm. The wound was cleaned with sterile 0.9% NaCl and closed by suture. Medication was performed as described above.

Histology

At the end of experiment or appropriate time-point, animals were deeply anesthetized by an intraperitoneal injection of sodium pentobarbital (50 mg/kg) and perfused with either 0.9% NaCl (ocular dominance experiment) or Na₂HPO₄·2H₂O (Acan-loxP CreNes) buffer, followed by 4% paraformaldehyde (PFA). Brains were dissected out and post fixed in PFA solution overnight and cryoprotected in 30% sucrose in 1x PBS for 24 hours. Coronal sections of 30 or 40µm were collected from the cryostat or freezing microtome and transferred to 1X PBS. Sections were rinsed in 1x PBS and blocked for 1 hour in 2-10% animal serum (species dependent on secondary antibody host) before primary antibody incubation overnight in blocking solution (Table 2). The following day, sections were rinsed and incubated with secondary antibodies for 2 hours. Sections were rinsed and mounted on Superfrost slides with FluorSave™ Reagent (Merck Millipore, Germany).

Following ocular dominance testing of AAV9.Cre injected Acan-loxP^{+/+} mice wide-field fluorescence images were acquired with an AxioPlan 2 (Zeiss, Germany) microscope through a 10x objective, and high-resolution overview images stitched using the Mosaix extension in the AxioVision software. Confocal images were acquired using a FluoView FV1000, software version 1.7 (Olympus), through a 20x or 60x PlanApo objective. Image analysis was performed using ImageJ (NIH) and Photoshop CS4/6 (Adobe).

For histological quantification of 3-4 month-old Acan-loxP^{+/+} x CreNes crosses images were captured using a Leica SPE confocal microscope using either x10 or x63 objectives with a 1024 x 1024 image resolution (n=3 per group). For PNN quantification at least 5 images per section (3 sections per brain, approximately 300µm apart) were taken on a single confocal plane in layers 4 and 5 of the mouse barrel cortex (Fig. 2). Images contained at least one WFA labelled PNN (if detected). For Acan-loxP^{+/+} CreNes, where no PNNs were detected, representative images were captured randomly in the same region. For PV cell analysis by immunohistochemistry at least 5 z-stack images (10 stacks, ~3µm apart) were taken per section with at least 5 sections analyzed per animal (approx. 300µm apart). Images were then analyzed with an automated custom script using the EBImage package from R statistical software (Pau et al.,

2010). To reduce variance in antibody binding all groups used for quantification were histologically stained in batches using the same conditions and antibody solutions.

Protein and RNA analysis

For aggrecan protein and gene expression analysis, snap frozen Acan-*loxP*^{+/+} and CreNes Acan-*loxP*^{+/+} brains (n = 3 per group) were homogenized over ice and both protein and RNA was extracted using an AllPrep DNA/RNA/protein Mini Kit (Qiagen, NL). Prior to aggrecan protein quantification 20µg brain homogenate from each sample was de-glycosylated with chondroitinase ABC in PBS with acetic acid (50U/ml, pH7.8) for 24hrs at 37°C to remove GAG side chains from the aggrecan core protein. Following de-glycosylation samples were subjected to a sodium dodecyl sulfate polyacrylamide gel electrophoresis (SDS-PAGE) method using a 4-12% Bis-Tris Mini Gel (NuPAGE, Invitrogen, USA) and Western blotting protein transfer to a PVDF membrane. Membranes were left to air dry before being washed three times with 2% Triton X-100 in Tris buffer solution (TBS-T). After the final wash, membranes were incubated in a blocking buffer (10% skimmed milk made in TBS-T) for 1 hour. After blocking, membranes were then incubated in primary antibodies overnight at 4°C with 5% skimmed milk in TBS-T. The following morning, membranes were washed in triplicate in TBS-T and incubated in secondary antibody for 1 hour, after which they were washed again. Proteins were then visualized using the electrochemiluminescence (ECL) method. Protein quantification was achieved using ImageJ comparing aggrecan signal intensity relative to β-actin. For aggrecan all bands >250kd were included for analysis similar to previous studies (Miyata and Kitagawa, 2016) while β-actin produced a clear band at 37kd.

For gene expression analysis mRNA was converted to single stranded cDNA using a High-Capacity cDNA Reverse Transcription Kit with RNase Inhibitor (Applied Biosystems, USA). Samples were then analyzed using quantitative PCR with inventoried TaqMan probes (Applied Biosystems, USA) for *Acan* and *Actb*. A final concentration of 14ng of cDNA per reaction was used. All samples were run in triplicate and averaged prior to analysis. Measurements for the expression of *Acan* were then presented relative to *Actb* for graphing and statistical analysis.

Table 2: Antibodies used to label PNN components and PV+ cells

Primary antibodies				
Reactivity	Host species	Supplier	cat #	RRID
N-acetylgalactosamine	n.a. (lectin)	Sigma	L-1516	AB_2620171
Aggrecan	Rabbit	Millipore	ab1031	AB_90460
Crtl-I	Mouse	Millipore	MABT85	AB_11203324

Ctrl-I	Goat	R&D	af2608	AB_2116135
GFP	Chicken	Life	ab13970	AB_300798
Neurocan	Sheep	Thermo	PA5-47779	AB_2608508
Versican	Rabbit	BosterBio	PB9453	not registered
Brevican	Mouse	BioLegend	820101	AB_2564837
tenascinR	Mouse	R&D	MAB1624	AB_2207001
Parvalbumin	Goat	Swant	PVG-214	AB_2313848
Parvalbumin	Rabbit	Swant	PV27	AB_2631173
Secondary used in biotin-tagging				
anti-mouse	Goat	Life	A-24522	AB_2535991
anti-goat	Donkey	abcam	ab6884	AB_954842
anti-rabbit	Goat	Life	31820	AB_228340

Quantification and statistics of the histology signal

Prior to image processing a 30% threshold was applied to the image to eliminate non-specific binding. Cells whose soma were in the Z-stack image were extracted and combined intensity values for all pixels in a cell were averaged and cropped images of PV positive cells were saved for manual verification. The AU scale was derived as before based on mean PV values extracted from the WT group.

Assessing OD plasticity in visual cortex using optical imaging of intrinsic signal

Visual stimulus was generated in Matlab using the Psychophysics toolbox, and presented on a 27.5 x 34 cm computer monitor (Dell Computers, 60 Hz refresh rate) placed 25 cm from the mouse. The stimulus consisted of a thin drifting bar (2° wide) moving up or down with temporal frequency of 0.17 Hz and spatial frequency of 0.05 cycles per degree. The stimulus was repeated 20 times, each presentation interleaved with a grey blank screen. The duration of each recording was 120 seconds. Stimulus was restricted to the binocular field of vision (20°), with an offset of 5° towards the respective open eye.

Eight to ten weeks after virus injection the animals were prepared for imaging. The experimenter performing imaging experiments and analysis was blind to treatment group and genotype. A custom steel plate for head fixation was attached to the skull using cyanoacrylate and dental acrylic, leaving the area above the visual cortex open. This was covered by a thin layer of nitrocellulose (New-Skin) to prevent desiccation and reactive cell growth.

207 After head plate implantation, the first imaging of intrinsic signals was performed to measure baseline
 208 responses through each eye. Repeated optical imaging of intrinsic signals was performed as described
 209 (Kaneko et al., 2008). The mouse was anesthetized with isoflurane (2% for induction and 0.5% during
 210 recording) supplemented with an intramuscular injection of chlorprothixene (2mg/kg body weight). The
 211 mice were head fixed and placed on a heating pad in front of the computer monitor and images were
 212 recorded transcranially by a Teledyne Dalsa M30P camera (Teledyne, CA, USA) using two adjacently
 213 mounted Nikon 50mm 1.2 lenses, and custom Matlab software. Light was provided by LED lights
 214 mounted in a ring surrounding the camera lens. Two 525nm LEDs were used to focus on the surface
 215 blood vessels before focus was shifted 600 μm below the surface. The light source was switched to three
 216 615 nm LED lights (XPEBRO-L1-R250-00B02 from Cree Inc., NC, USA) and emission light was filtered
 217 with a red interference filter (610 ± 10 nm). Images were acquired with a frame rate of 30 fps. The phase
 218 and amplitude of cortical responses at the stimulus frequency were extracted by Fourier analysis as
 219 described (Kalatsky and Stryker, 2003). The responses to stimulation of each of the eyes were recorded
 220 for 4-6 trials, alternating between which eye was covered. The median of the peak response amplitude (R)
 221 of all trials for each eye were used to calculate an ocular dominance index (ODI) by $\text{ODI} = (\text{R}^{\text{contra}} - \text{R}^{\text{ipsi}}) /$
 222 $\text{R}^{\text{contra}} + \text{R}^{\text{ipsi}}$.

223 Immediately after baseline imaging, the eyelids to the contralateral eye was sutured shut. Lidocaine was
 224 applied to the sutured area and the animal returned to its home cage. After four days, the mice were again
 225 anesthetized, the closed eyelid was re-opened and the imaging procedure repeated as described above.

226

227 Assessing memory by spontaneous object recognition behavioral task

228 In order to gauge memory ability of Acan-loxP^{+/+} Cre mice, a Spontaneous Object Recognition (SOR)
 229 behavioral task was used. During testing, male mice ($n = >7$ per group, approximately 3 months old) were
 230 placed individually in a Y-shaped maze (30cm high, all arms 16cm in length and 8cm wide) as previously
 231 described (Romberg et al., 2013). Briefly, animals were habituated to the testing arena for two
 232 consecutive days prior to testing where animals were allowed to explore freely for 5 minutes each day.
 233 Each testing session occurred during the dark phase and consisted of a sample phase and a choice phase,
 234 using the same objects as in Romberg et al. 2013. During the sample phase, a mouse was placed in the
 235 start arm of the maze with sample objects (two identical objects) placed in the two remaining arms and
 236 left to explore the objects freely for 5 minutes. After a 3 hours or 24 hour delay animals were returned to
 237 the maze for the choice phase. During the choice phase two new objects were placed in the sample arms,

one that is the same as the sample objects (familiar object) and one that was new to the mouse (novel object). For each delay time, mice underwent at least one testing session. All testing sessions were separated by a minimum of 48hrs to allow recuperation. The presentation of the object pairs and their appearance in either the left or right sample arm were counterbalanced so that a particular object in a set or a particular side might be novel for one animal and not for another to avoid unforeseen bias. The maze and all objects were wiped down with 70% EtOH in between each testing session in order to avoid any olfactory bias that could have been introduced during the previous testing session. Time spent exploring each object during the sample and choice phase was assessed and scored at a later date using the video recordings. A discrimination score was calculated for the choice phase by subtracting the amount of time exploring the familiar object from the amount of time exploring the novel object and then dividing by the total exploration time:

$$\frac{\text{Time exploring novel} - \text{Time exploring familiar}}{\text{Time exploring novel} + \text{Time exploring familiar}}$$

A positive score indicates recognition of the novel object, while a score of 0 or below indicates the mouse was unable to recognize the novel object. An average was taken for the total sample times per object and the discrimination scores for the choice per time delay.

252

253 EXPERIMENTAL DESIGN AND STATISTICAL ANALYSIS

Statistical analysis was performed using R (R Foundation) or GraphPad Prism 7 (Graphpad Software, CA, USA). Datasets were tested for normality using Shapiro-Wilk's test or Fisher's F test. Comparisons between two groups were tested by Welch's t-test or paired t-test. Multiple group analysis was achieved using a type 1 or type 3 ANOVA with the appropriate follow up test, either post hoc Tukey HSD or comparing two groups by Welch's t-test.

Biochemical quantification of aggrecan protein and the Acan transcript were conducted as described in the *Protein and RNA analysis* paragraph above. Separate brain homogenates from 3 male animals, 3-4 months of age from litters originating from the same breeding pair, belonging to each of the 2 experimental groups; Acan-loxP^(+/+) and Acan-loxP^(+/+)Cre, were analyzed. For protein quantification ImageJ was used to quantify aggrecan signal which was normalized to β-actin signal, each lane corresponding to an individual animal (Fig. 1d). For mRNA quantification triplicates of 14 ng cDNA derived from each of the individual animals were run with TaqMan probes against *Acan* and *Actb*, and the relative signal was quantified by the accompanying software (Fig. 1e). The 2 experimental groups were compared and tested in a Welch's t-test.

268 Table 3: Statistical analysis biochemical quantification

Welch Two Sample t-test				
	<u>T</u>	<u>Df</u>	<u>p-value</u>	<u>mean of x, mean of y</u>
Ab1031 WB	11.365	2.7346	0.002216 **	1.7059754, 0.7572072
qPCR	5.501	2.0556	0.02963 *	0.7260774, 0.1914709
Signif. codes: '****' 0.001 '***' 0.01 '**' 0.05				

269

270 *Quantification of PNN intensity by WFA and Aggrecan immunohistochemistry* were conducted as
 271 described in the *Histology* paragraph above. There were 3 male animals of 3-4 months of age originating
 272 from the same lines of breeding in each of the 3 experimental groups; WT, Acan-loxP^(+/+) and Acan-
 273 loxP^(+/-)Cre. At least 5 images from each of 3 sections from each brain of the individual animals were
 274 analyzed. Images were analyzed with an automated custom script using the EBImage package from R
 275 statistical software (Pau et al., 2010). For each experimental group, more than 150 and 50 PNN structures
 276 where quantified respectively by WFA and aggrecan histochemistry. Each PNN structure is represented
 277 as a dot in Figure 2b and 2c. The 3 experimental groups were tested in One-way ANOVA with a
 278 TukeyHSD post hoc test.

279 **Table 4: Statistical analysis quantification of PNN intensity**

Anova - WFA					
	Df	Sum Sq	Mean Sq	F value	Pr(>F)
Group	2	0.234	0.1170	8.419	0.000244 ***
Residuals	695	9.660	0.0139		
Signif. codes: 0 '****' 0.001 '***' 0.01 '**' 0.05 '.' 0.1 ' ' 1					
Tukey multiple comparisons of means - WFA 95% family-wise confidence level					
	Diff	Lwr	upr	p adj	

tghetcre-tg	-0.04293423	-0.06804163	-0.01782683	0.0001934	
wt-tg	-0.01396332	-0.04019866	0.01227202	0.4241323	
wt-tghetcre	0.02897091	0.00310826	0.05483356	0.0236190	
Anova - Aggrecan					
	Df	Sum Sq	Mean Sq	F value	Pr(>F)
Group	2	0.082	0.04100	4.676	0.0104 *
Residuals	192	1.683	0.00877		
Signif. codes: 0 ‘****’ 0.001 ‘***’ 0.01 ‘**’ 0.05 ‘.’ 0.1 ‘ ’ 1					
Tukey multiple comparisons of means – Aggrecan 95% family-wise confidence level					
	Diff	lwr	upr	p adj	
tghetcre-tg	-0.041990928	-0.08357968	-0.0004021726	0.0472421*	
wt-tg	0.009533334	-0.02685560	0.0459222690	0.8100014	
wt-tghetcre	0.051524262	0.01058598	0.0924625400	0.0092913**	

280

281 *Quantification of PV intensity by PV immunohistochemistry* was conducted as described in the *Histology*
 282 paragraph above. There were 3 male animals of 3–4 months of age originating from same lines of
 283 breeding, in each of the 4 experimental groups; WT, Acan-loxP^(+/+), Acan-loxP^(+/-)Cre, and Acan-
 284 loxP^(+/+)Cre. 5 z-stack images, each consisting of 10 individual images 3 μ m apart, were taken from each
 285 of 5 sections from each brain of the individual animals and analyzed. Images were analyzed with an
 286 automated custom script using the EBImage package from R statistical software (Pau et al., 2010). More
 287 than 150 PV positive cells were quantified for each experimental group and represented as a dot in Figure
 288 2f. The 4 experimental groups were tested in One-way ANOVA with a TukeyHSD post hoc test.

289 **Table 5: Statistical analysis quantification of PV**

Anova - PV					
	Df	Sum Sq	Mean Sq	F value	Pr(>F)

Group	3	6.65	2.2169	39.53	<2e-16 ***
Residuals	1160	65.05	0.0561		
Signif. codes: 0 '***' 0.001 '**' 0.01 '*' 0.05 '.' 0.1 ' ' 1					
Tukey multiple comparisons of means – PV 95% family-wise confidence level					
	diff	lwr	upr	p adj	
tgcre-tg	-0.09178599	-0.149596189	-0.033975795	0.0002750***	
tghetcre-tg	-0.16498059	-0.228473244	-0.101487941	0.0000000****	
wt-tg	0.04478937	-0.002047122	0.091625869	0.0668269	
tghetcre-tgcre	-0.07319460	-0.138715560	-0.007673641	0.0214535*	
wt-tgcre	0.13657537	0.087024012	0.186126719	0.0000000****	
wt-tghetcre	0.20976997	0.153692925	0.265847008	0.0000000****	

290

291 *Quantification of PNN intensity by WFA after local removal of Acan* was conducted as described in the
 292 *Histology* paragraph above. There were 6 male animals (3-4 months) originating from different litters but
 293 from the same breeding pair in which each of the two hemispheres contributed to 2 experimental groups;
 294 Controlateral control and AAV9.Cre injected hemispheres. 3 sections from each of the individual animals
 295 were imaged. Each of the hemispheres of the individual animals is represented as a dot in Figure 3c. The
 296 2 experimental groups were tested in a paired t-test. Results are stated in the legend of figure 3.

297 *Assessing OD plasticity* was conducted as described in the *Assessing OD plasticity in visual cortex using*
 298 *optical imaging of intrinsic signal* paragraph above. There were 4, 3, and 7 male animals aged 5-7 months
 299 originating from the same line two breeding pairs and some from the same litters in the 3 different
 300 experimental groups; Acan-loxP^(+/+) untreated, Acan-loxP^(+/-) AAV9.Cre injected, and Acan-loxP^(+/+)
 301 AAV9.Cre injected. Responses to visual stimuli by each of the two eyes were recorded in 4-6 trials per
 302 eye. Each trial consisted of 20 repetitions of a visual stimulus of 120 seconds with simultaneous imaging
 303 of the cortex. Initially, baseline responses by the two individual eyes and corresponding ODI for all
 304 animals were determined (Fig. 1c, d and e). Filled colored circles indicate population means while open
 305 grey circles indicate individual animals. After MD of 4 days, the trials were repeated. Eye responses and
 306 ODI are represented in similar fashion. A shift in eye responses and ODI induced by MD of 4 day were
 307 tested in a paired t-test within the 3 experimental groups, or with Wilcoxon signed rank test if the
 308 distribution was not normal. Results are stated in the legend of figure 4.

309 *Assessing memory of spontaneous object recognition* was conducted as described in the *Assessing*
 310 *memory by spontaneous object recognition behavioral task* paragraph above. There were 7, 9 (which of
 311 one was singly housed), 10 and 7 male animals of ~3 months of age originating same line of breeding in

each of the 4 experimental groups; WT, Acan-loxP^(+/+), Acan-loxP^(+/-)Cre, and Acan-loxP^(+/+)Cre. Average exploration times for all experiments in each of the experimental groups varied between 40 and 50 seconds (Fig. 5b). To assess differences in the ability to retain memory (Fig. 5c) Anova was used to compare variances between the groups prior to engaging in post hoc analysis. A significant difference was found in the timepoint variable which then justified the exploration of the timepoint differences within groups and reduced the likelihood that significant values were reached through chance.

Table 6: Statistical analysis spontaneous object recognition task

Anova Table (Type III tests) – SOR				
	<u>Sum Sq</u>	<u>Df</u>	<u>F value</u>	<u>Pr(>F)</u>
(Intercept)	1.10135	1	74.7174	3.939e-12 ***
Timepoint	0.45081	1	30.5840	7.362e-07 ***
Residuals	0.88441	60		
Welch Two Sample t-tests – SOR timepoint				
3hr v 24hr	T	Df	p-value	mean of x, mean of y
WT	2.5638	11.555	0.02547 *	0.291830, 0.127394
Homo	4.326	11.201	0.001154 **	0.27991577, 0.07462545
Het	2.7797	12.071	0.01658 *	0.26169284, 0.08900274
HomoCre	0.92565	9.832	0.3768	0.2668251, 0.2013353
Signif. codes: '****' 0.001 '***' 0.01 '**' 0.05				

RESULTS

This mouse model was established by acquiring JM8A3.N1 ES cells (Pettitt et al., 2009) carrying the “knockout-first” conditional *tmla* (Fig. 1a) from the European Mouse Mutant Cell Repository (EuMMCR) (Skarnes et al., 2011). The initial strain was subsequently converted to B6(Cg)-ACAN^{tmlc(EUCOMM)Hmgu>/Jwfa} hereafter referred to as Acan-loxP, where Cre recombinase induces an exon deletion and a frame-shift mutation in *Acan* (Fig. 1a).

Brain-wide targeting of *Acan* was achieved by crossing Acan-loxP with Nestin-CRE (CreNes) where Cre recombinase is expressed under the control of the promoter and the nervous system-specific enhancer present in the second intron of the rat *Nes* gene (Tronche et al., 1999).

Targeting aggrecan in the brain of Acan-loxP^{+/+} CreNes mice was accompanied by complete loss of histochemical staining of PNNs in the cortex using the PNN marker *Wisteria floribunda agglutinin* (WFA) (Fig. 1b). Ablation of aggrecan was verified by immunohistochemistry and western blotting (Fig. 1c, d) and reduced *Acan* mRNA in the brain (Fig. 1e). In these animals PNNs detected by WFA were absent in the brain. The loss of aggrecan prevented aggregation of other PNN component ECM molecules into PNNs, effectively abolishing PNNs in the adult cortex (Fig. 1f, representative example from > 50 images per PNN component. Fig. 2a, overview of sampling). In contrast, the non-targeted Acan-loxP^{+/+} mice with two intact alleles expressing *Acan*, and the targeted heterozygous Acan-loxP^{+/-} CreNes mice having one intact allele, both had anatomically normal PNNs (Fig. 1b, f), although the intensity of the WFA staining was reduced in the heterozygote (Fig. 2b-e). The crucial dependence of aggrecan for PNN formation is in line with previous results from *in vitro* models demonstrating that aggrecan, link protein and hyaluronic acid are essential components of net formation and stability (Giamanco et al., 2010; Kwok et al., 2010). In contrast, knock-out of the link protein Ctrl1 has been shown to give only a partial reduction of WFA-positive PNNs (Carulli et al., 2010).

A shift in the distribution of WFA histochemical labeling intensity has been suggested to correlate with the degree of neuronal plasticity in learning and memory (Balmer et al., 2009). Recently, parvalbumin (PV) expression on GABAergic interneurons has been shown to be influenced by PNNs in the hippocampus (Yamada et al., 2015), and the differentiation state and activity of PV+ interneurons relate to learning and memory formation (Donato et al., 2013). To assess if the reduction or complete lack of aggrecan affects the local PV expression, z-stacked images were acquired, and mean PV intensities of neurons in somatosensory cortex were extracted (> 150 cells per group, 3- 6 sections per group). In both the heterozygous Acan-loxP^{+/-} CreNes mice and homozygous Acan-loxP^{+/+} CreNes mice there was a shift towards lower PV expression by PV+ interneurons in the cortex compared to wild type and Acan-loxP^{+/+}

controls (Fig 2f-h), indicating that even partial attenuation of the *Acan* gene induces a low-PV state. This suggests that *Acan-loxP^{+/+}-CreNes* mice are in a state of high network plasticity.

To investigate the effect of locally removing aggrecan in the adult mouse brain, *Acan* was targeted by injecting the viral vector AAV9.hSyn.HI.eGFP.WPRE.SV40 (AAV9.Cre) carrying Cre recombinase into the primary visual cortex (V1) (Fig. 3a). The synapsin promoter restricted expression to neurons. Local injections of AAV9.Cre in adult *Acan-loxP^{+/+}* mice caused a complete loss of aggrecan and WFA labeling in V1 eight weeks after virus injection (Fig. 3b, c). The combined expression of GFP and Cre by the virus revealed loss of PNNs surrounding infected neurons, demonstrating that expression of aggrecan by neurons is needed to form the PNN structure. Again, loss of aggrecan disrupted aggregation of the other PNN components (Fig. 3e), suggesting that aggrecan is essential for sustaining PNNs in the visual cortex. Together, these targeting experiments demonstrate an essential role for aggrecan in PNN formation.

PNNs have been implicated in limiting adult brain plasticity due to their; CS content (Pizzorusso et al., 2002; Miyata et al., 2012), enclosing mesh structure (Carulli et al., 2010), ability to bind and sequester active molecules (Beurdeley et al., 2012; Dick et al., 2013), and role in controlling (Kwok et al., 2011) the activity of fast spiking PV positive neurons (Balmer, 2016; Lensjo et al., 2017). Although several PNN CSPGs have been linked to plasticity regulation, the role of aggrecan, the backbone of PNN remains to be investigated, and a full picture of plasticity regulation is lacking. Activity-dependent plasticity was assessed by inducing ocular dominance (OD) plasticity in the binocular region of primary visual cortex (V1) of adult mice using monocular deprivation (MD). Tracing of the connections between the lateral geniculate nucleus and V1 revealed normal retinotopic connectivity between V1 and lateral geniculate nucleus in the thalamus in the non-targeted *Acan-loxP^{+/+}* animal (Fig. 4a). Visual responses before and after MD were recorded using optical imaging of intrinsic signals (Fig. 4b), and all groups displayed robust responses to visual stimuli (more than 2x the response compared to during grey screen presentations) before MD (Fig 4d, “baseline”). Strikingly, four days of MD were sufficient to produce a strong and significant shift in OD in adult AAV9.Cre injected *Acan-loxP^{+/+}* mice, while no effect was observed in AAV9.Cre injected *Acan-loxP^{+/-}* mice or non-injected *Acan-loxP^{+/+}* mice (Fig. 4c). Longer lasting sensory deprivation has been shown to induce some OD plasticity also in adult mice, but the mechanism differs from juvenile plasticity (Sawtell et al., 2003; Ranson et al., 2012). To determine if PNN removal caused enhanced adult plasticity or instead reinstated juvenile plasticity, the responses to stimulation of each eye before and after MD were investigated. We did not see the adult OD plasticity

pattern, characterized by strengthening of ipsilateral input to V1. Instead, the shift in OD was driven both by a potentiation of ipsilateral responses and a reduction in contralateral responses, indicating plasticity mechanisms similar to juvenile animals (Fig. 4d). No significant effects were observed in non-injected Acan-loxP^{+/+} mice or AAV9.Cre injected Acan-loxP^{+/-} mice (Fig. 4d).

Several interventions affecting PNNs have effects on learning and memory (Gogolla et al., 2009; Carulli et al., 2010; Romberg et al., 2013). The effect of brain-wide knockdown of aggrecan in learning and memory behavior was tested in the spontaneous object recognition paradigm (Romberg et al., 2013). In this paradigm, depicted in figure 5a, animals (> 7 per group) identify novel from familiar objects (choice phase) following a delay from familiar object presentation (sample phase). Animals were tested after three and 24 hour delays, at which times ChABC-treated and Crt11 knockout animals show enhanced memory retention (Romberg et al., 2013). Following the three hours delay between sample and choice phases, all groups displayed a good ability to recognize the novel from familiar objects (discrimination ratio > 0.25). At 24 hours of the sample phase, the wild type, Acan-loxP^{+/+} and Acan-loxP^{+/-} CreNes groups (Fig. 5c) showed little remaining memory. Remarkably, the object recognition memory in the Acan-loxP^{+/+} CreNes group was still sustained at 24 hours after object exposure (Fig. 5c), indicating a stronger recognition memory in mice lacking aggrecan. These results are very similar to those obtained after ChABC treatment and in Crt11 knockouts, suggesting that the Acan knockout affects memory through effects on glycan chains in PNNs. Although heterozygous Acan-loxP^{+/-} CreNes have reduced PNNs intensity and altered PV expression, alterations in their behavior were not detected.

DISCUSSION

It has been suggested that aggrecan-containing PNNs play an essential role in regulation of brain plasticity. However, the hypothesis has been difficult to test directly due to technical limitations such as the off-target effects of the PNN-degrading enzyme Chondroitinase ABC and the dependence on intact aggrecan for cartilage formation. In the current work, we established a conditional knock-out model for aggrecan and demonstrate that aggrecan is indeed required for the aggregation of PNNs and that its removal reopens juvenile plasticity in visual cortex and affects memory processing. This work reveals that aggrecan is essential for PNN formation *in vivo*, and specific loss of PNNs increase adult brain plasticity.

PNNs probably control synaptic plasticity and dynamics through several mechanisms. Most of these

depend on the actions of the sulfated CSPG glycosaminoglycan chains attached to the several CSPGs that populate PNNs (Sorg et al., 2016), selective binding and facilitated internalization of the homeobox transcription factor OTX2 which affects maturation of PV⁺ interneurons (Beurdeley et al., 2012), binding and presentation of chemorepulsive semaphorin3A (Dick et al., 2013), and regulation of AMPA receptor mobility (Frischknecht et al., 2009). These mechanisms are based on the distinctive PNN structure; the tight cross-linking structures of matrix proteins, CS and hyaluronic acid polysaccharides forming a condensed compact matrix surrounding the cell soma and proximal dendrites, and the ability of the negatively charged sulfation patterns of the CS to allow specific interactions with positively charged domains in PNN interacting proteins. Indeed, the ratio of 4- and 6-sulfated CS influences neuronal plasticity (Miyata et al., 2012). Our data suggest that aggrecan plays a key role for the PNN structure, possibly through the large number of glycan chains that it carries, but clearly by affecting formation. Removal of aggrecan abolishes aggregation of PNNs, and essentially also incorporation of other ECM components into the structure (Fig 1 and 3). Aggrecan is an efficient cross-linker interacting with hyaluronic acid and link protein by its N-terminal G1 domain and the extensively CS GAG modified central domain (Morawski et al., 2012). The three globular domains; G1, G2 and G3 interact with several matrix molecules aiding cross-linking, which could explain the failure of other components to aggregate in its absence. The increased plasticity after PNN removal could also be a direct consequence of neuronal activity changes in PV⁺ cells. This has been shown to be an important factor in regulation of CP plasticity (Hensch, 2004), and previous work has shown that PNN removal reduces the activity of PV⁺ neurons (Balmer, 2016; Lensjo et al., 2017). The changes in activity could be a result of reduced ion buffering, changes to the synaptic inputs onto PV⁺ cells, alteration within the PV cells due to changed interaction with external molecular cues, or a combination of these.

Condensation of PNNs in sensory cortices correlates with closure of periods of heightened neuronal plasticity in sensory systems. Our results show that monocular deprivation induces a strong and rapid change in cortical activation in V1 after just four days of MD. The timeframe of this shift is faster than what has been observed in CP aged mice (Sato and Stryker, 2008), but is in line with previous work on adult mice with induced plasticity (Fu et al., 2015). While monocular deprivation in adults normally effects only responses to ipsilateral eye stimulation, we observed changes in responsiveness to both contra- and ipsilateral inputs to V1 (Fig. 4), similar to how this shift occurs in CP aged animals. This finding is supported by our recent work which showed that brief MD in adult rats following enzymatic degradation of PNNs caused a similar effect on recorded single units in V1, in both hemispheres relative to the

deprived eye (Lensjo et al., 2017). These effects differ from other manipulations to activate adult cortical plasticity such as Lynx1 deletion (Morishita et al., 2010), which arises as a result of potentiated responses to ipsilateral stimuli. Taken together, this suggest that the PNN is a determinant factor in closure of the CPs in juvenile development, through its effect on PV+ neurons and action as a structural barrier. Removal of aggrecan collapses the PNN structure and leads to a persistent state of juvenile-like plasticity.

Our data also show that populations of PV+ interneurons in both homozygous and heterozygous Acan-loxP^{+/+}-CreNes mice are shifted to a state where they express less PV (Fig. 2). Others have suggested that the level of PV in PV+ interneurons determine if the network is in a state of high or low plasticity (Donato et al., 2013) through a mechanism involving gene expression of PV and the GABA-synthesizing enzyme GAD67 and regulation of the activity of the neurons through changes in dendritic synaptic contacts. Decreased PV expression and synapses are associated with hippocampal learning, while fear conditioning leads to a high-PV state. PV+ neuron-controlled shifts in network state are suggested as an integrated mechanism of learning and memory acquisition. ChABC treatment to degrade PNNs shifted the network to a low-PV state, indicating that the glycans on CSPGs are a key component in controlling PV interneuron influence on network state. Mounting evidence from other brain structures supports a broader role for PNNs where they affect behavior, memory and learning processes. We show that PNN removal by aggrecan knock-out improves object recognition memory (Fig. 5), in line with previous work (Romberg et al., 2013). Recently, aggrecan and PNNs have been implied in various psychiatric disorders (Pantazopoulos et al., 2015), and in the progression of neurodegenerative diseases (Suttkus et al., 2016). Subtle differences in matrix and PNN structure might impact the balance between a resilient and a susceptible and vulnerable state.

In the current study, the Acan-loxP mouse line has established a role for this CSPG in the control of plasticity in visual cortex and in memory. Aggrecan is the key component for assembling and sustaining the PNNs structure and function in the adult brain and may play a central role in regulating adult brain plasticity.

REFERENCES:

- Balmer TS (2016) Perineuronal Nets Enhance the Excitability of Fast-Spiking Neurons. *eNeuro* 3.
 Balmer TS, Carels VM, Frisch JL, Nick TA (2009) Modulation of perineuronal nets and parvalbumin with developmental song learning. *J Neurosci* 29:12878-12885.
 Beurdeley M, Spatazza J, Lee HH, Sugiyama S, Bernard C, Di Nardo AA, Hensch TK, Prochiantz A (2012) Otx2 binding to perineuronal nets persistently regulates plasticity in the mature visual cortex. *J Neurosci* 32:9429-9437.
 Carulli D, Pizzorusso T, Kwok JC, Putignano E, Poli A, Forostyak S, Andrews MR, Deepa SS, Glant TT, Fawcett JW (2010) Animals lacking link protein have attenuated perineuronal nets and persistent plasticity. *Brain* 133:2331-2347.

- Deepa SS, Carulli D, Galtrey C, Rhodes K, Fukuda J, Mikami T, Sugahara K, Fawcett JW (2006) Composition of perineuronal net extracellular matrix in rat brain: a different disaccharide composition for the net-associated proteoglycans. *The Journal of biological chemistry* 281:17789-17800.
- Dick G, Tan CL, Alves JN, Ehler EM, Miller GM, Hsieh-Wilson LC, Sugahara K, Oosterhof A, van Kuppevelt TH, Verhaagen J, Fawcett JW, Kwok JC (2013) Semaphorin 3A binds to the perineuronal nets via chondroitin sulfate type E motifs in rodent brains. *J Biol Chem* 288:27384-27395.
- Donato F, Rompani SB, Caroni P (2013) Parvalbumin-expressing basket-cell network plasticity induced by experience regulates adult learning. *Nature* 504:272-276.
- Frischknecht R, Heine M, Perrais D, Seidenbecher CI, Choquet D, Gundelfinger ED (2009) Brain extracellular matrix affects AMPA receptor lateral mobility and short-term synaptic plasticity. *Nat Neurosci* 12:897-904.
- Fu Y, Kaneko M, Tang Y, Alvarez-Buylla A, Stryker MP (2015) A cortical disinhibitory circuit for enhancing adult plasticity. *Elife* 4:e05558.
- Giamanco KA, Morawski M, Matthews RT (2010) Perineuronal net formation and structure in aggrecan knockout mice. *Neuroscience* 170:1314-1327.
- Gogolla N, Caroni P, Luthi A, Herry C (2009) Perineuronal nets protect fear memories from erasure. *Science* 325:1258-1261.
- Hartig W, Brauer K, Bigl V, Bruckner G (1994) Chondroitin sulfate proteoglycan-immunoreactivity of lectin-labeled perineuronal nets around parvalbumin-containing neurons. *Brain Res* 635:307-311.
- Hensch TK (2004) Critical period regulation. *Annual review of neuroscience* 27:549-579.
- Kalatsky VA, Stryker MP (2003) New paradigm for optical imaging: temporally encoded maps of intrinsic signal. *Neuron* 38:529-545.
- Kaneko M, Stellwagen D, Malenka RC, Stryker MP (2008) Tumor necrosis factor- α mediates one component of competitive, experience-dependent plasticity in developing visual cortex. *Neuron* 58:673-680.
- Kwok JC, Carulli D, Fawcett JW (2010) In vitro modeling of perineuronal nets: hyaluronan synthase and link protein are necessary for their formation and integrity. *J Neurochem* 114:1447-1459.
- Kwok JC, Dick G, Wang D, Fawcett JW (2011) Extracellular matrix and perineuronal nets in CNS repair. *Dev Neurobiol* 71:1073-1089.
- Lensjo KK, Lepperød ME, Dick G, Hafting T, Fyhn M (2017) Removal of Perineuronal Nets Unlocks Juvenile Plasticity Through Network Mechanisms of Decreased Inhibition and Increased Gamma Activity. *J Neurosci* 37:1269-1283.
- Matthews RT, Kelly GM, Zerillo CA, Gray G, Tiemeyer M, Hockfield S (2002) Aggrecan glycoforms contribute to the molecular heterogeneity of perineuronal nets. *The Journal of neuroscience : the official journal of the Society for Neuroscience* 22:7536-7547.
- Miyata S, Kitagawa H (2016) Chondroitin 6-Sulfation Regulates Perineuronal Net Formation by Controlling the Stability of Aggrecan. *Neural plasticity* 2016:1305801.
- Miyata S, Komatsu Y, Yoshimura Y, Taya C, Kitagawa H (2012) Persistent cortical plasticity by upregulation of chondroitin 6-sulfation. *Nat Neurosci* 15:414-422, S411-412.
- Morawski M, Bruckner G, Arendt T, Matthews RT (2012) Aggrecan: Beyond cartilage and into the brain. *The international journal of biochemistry & cell biology* 44:690-693.
- Morishita H, Miwa JM, Heintz N, Hensch TK (2010) Lynx1, a cholinergic brake, limits plasticity in adult visual cortex. *Science* 330:1238-1240.
- Pantazopoulos H, Markota M, Jaquet F, Ghosh D, Wallin A, Santos A, Caterson B, Berretta S (2015) Aggrecan and chondroitin-6-sulfate abnormalities in schizophrenia and bipolar disorder: a postmortem study on the amygdala. *Translational psychiatry* 5:e496.
- Pau G, Fuchs F, Sklyar O, Boutros M, Huber W (2010) EBIImage--an R package for image processing with applications to cellular phenotypes. *Bioinformatics* 26:979-981.
- Pettitt SJ, Liang Q, Rairdan XY, Moran JL, Prosser HM, Beier DR, Lloyd KC, Bradley A, Skarnes WC (2009) Agouti C57BL/6N embryonic stem cells for mouse genetic resources. *Nature methods* 6:493-495.
- Pizzorusso T, Medini P, Berardi N, Chierzi S, Fawcett JW, Maffei L (2002) Reactivation of ocular dominance plasticity in the adult visual cortex. *Science* 298:1248-1251.
- Ranson A, Cheetham CE, Fox K, Sengpiel F (2012) Homeostatic plasticity mechanisms are required for juvenile, but not adult, ocular dominance plasticity. *Proc Natl Acad Sci U S A* 109:1311-1316.
- Rittenhouse E, Dunn LC, Cookingham J, Calo C, Spiegelman M, Dooher GB, Bennett D (1978) Cartilage matrix deficiency (cmd): a new autosomal recessive lethal mutation in the mouse. *J Embryol Exp Morphol* 43:71-

84.
 Romberg C, Yang S, Melani R, Andrews MR, Horner AE, Spillantini MG, Bussey TJ, Fawcett JW, Pizzorusso T, Saksida LM (2013) Depletion of perineuronal nets enhances recognition memory and long-term depression in the perirhinal cortex. *J Neurosci* 33:7057-7065.
 Sato M, Stryker MP (2008) Distinctive features of adult ocular dominance plasticity. *J Neurosci* 28:10278-10286.
 Sawtell NB, Frenkel MY, Philpot BD, Nakazawa K, Tonegawa S, Bear MF (2003) NMDA receptor-dependent ocular dominance plasticity in adult visual cortex. *Neuron* 38:977-985.
 Skarnes WC, Rosen B, West AP, Koutsourakis M, Bushell W, Iyer V, Mujica AO, Thomas M, Harrow J, Cox T, Jackson D, Severin J, Biggs P, Fu J, Nefedov M, de Jong PJ, Stewart AF, Bradley A (2011) A conditional knockout resource for the genome-wide study of mouse gene function. *Nature* 474:337-342.
 Sorg BA, Berretta S, Blacktop JM, Fawcett JW, Kitagawa H, Kwok JC, Miquel M (2016) Casting a Wide Net: Role of Perineuronal Nets in Neural Plasticity. *J Neurosci* 36:11459-11468.
 Suttkus A, Morawski M, Arendt T (2016) Protective Properties of Neural Extracellular Matrix. *Molecular neurobiology* 53:73-82.
 Tronche F, Kellendonk C, Kretz O, Gass P, Anlag K, Orban PC, Bock R, Klein R, Schutz G (1999) Disruption of the glucocorticoid receptor gene in the nervous system results in reduced anxiety. *Nat Genet* 23:99-103.
 Yamada J, Ohgomori T, Jinno S (2015) Perineuronal nets affect parvalbumin expression in GABAergic neurons of the mouse hippocampus. *Eur J Neurosci* 41:368-378.

Author contributions:

DR, KKL, TD, SY, MRA, TH, MF, JWF and GD designed and planned the experiments. MRA, JWF and GD initiated the work and together with MF developed the *Acan-loxP^{+/+}* mouse model. DR, KKL, MRA and GD performed breeding and genotyping. DR performed w.blot, qPCR, histology experiments and quantification of developmental and brain-wide knock-out of *Acan*. KKL performed histology and all surgical procedures in acute and local knock-out of *Acan*. TD performed monocular deprivation experiments assisted by TH and KKL. DR performed testing and analysis for behavioral experiments together with SY. MRA, MF, TH, JWF, and GD contributed with analysis and writing. The resulting manuscript was written by DR, KKL, MRA, TH, MF, JWF and GD.

FIGURES:

Fig. 1: Brain-wide targeting of the *Acan* gene results in abolition of WFA labelled PNNs and individual PNN components.

a: Schematic representation of the transgenic cassette designed by EuCOMMM; tm1a allele, containing exon 4 of the *Acan* gene, the subsequent conversion to tm1c by Flp-*FRT* recombination and the knock-out

allele tm1d by Cre-lox recombination. **b:** Representative image of cortical layers 1 – 6 from barrel cortex in wild type (WT), transgenic controls (Acan-loxP^{+/+}), heterozygous *Acan* knockout (Acan-loxP^{+/-}Cre) and homozygous *Acan* knockout (Acan-loxP^{+/+}Cre). Sections were stained with WFA (PNN marker, red) and DAPI (nuclear marker, blue), n = 3 per group and scale bar = 100μm. WT, Acan-loxP^{+/+} and Acan-loxP^{+/-}Cre mice appear to have similar numbers and disposition of PNNs, while a complete abolition of PNN staining was observed in Acan-loxP^{+/+}Cre brains. **c:** Representative examples of western blot of brain homogenates from Acan-loxP^{+/+} and Acan-loxP^{+/-}Cre mice using the polyclonal aggrecan antibody ab1031. **d:** Quantification of aggrecan protein. **e:** Quantification of *Acan* mRNA expression from Acan-loxP^{+/+} and Acan-loxP^{+/-}Cre mouse brains. **f:** Representative images of immunohistochemistry of aggrecan, brevican, neurocan, phosphacan, versican, tenascin-R (Tn-R), link protein 1 (Crtl1), and brain link protein 2 (Bral2) from WT, Acan-loxP^{+/+}, Acan-loxP^{+/-}Cre and Acan-loxP^{+/+}Cre mouse brains. For antibodies, see table in Materials and methods. ** = p < 0.01, * = p < 0.05, error bars are ± SEM.

Fig. 2: Partial and total removal of aggrecan affects PNN and PV interneuron properties. **a:** Coronal brain section from a wild type mouse showing the approximate locations in the barrel cortex used for histological sampling (labeled by *). Section stained the perineuronal net marker *Wisteria floribunda* agglutinin (WFA, red) and aggrecan (ab1031, green). Scale bar = 500μm. **b-e:** Mean intensity values of WFA-positive (**b**) or aggrecan-positive (**c**) PNNs in the cortex of WT (purple), Acan-loxP^{+/+} (blue) and Acan-loxP^{+/-}Cre (red) were extracted and analyzed. Acan-loxP^{+/-}Cre displayed a significant reduction in average WFA intensity and aggrecan intensity compared to WT and Acan-loxP^{+/+} controls. **f:** Mean intensity values of PV+ neurons in the cortex of WT (purple), Acan-loxP^{+/+} (blue), Acan-loxP^{+/-}Cre (red) and Acan-loxP^{+/+}Cre (green) were extracted and analyzed. Both Acan-loxP^{+/-}Cre and Acan-loxP^{+/+}Cre groups displayed a significant reduction in average mean intensity per PV+ cell compared to WT and Acan-loxP^{+/+} controls. Same cortical locations were used for PV histological sampling as depicted for WFA and Aggrecan in **a**. **g:** Examples of high, medium and low expressing PV neurons. **h:** Categorization of individual cells based on mean PV intensity indicated a shift towards a low PV network configuration in the Acan-loxP^{+/-}Cre and Acan-loxP^{+/+}Cre groups compared to controls.

Fig. 3: Targeted knock-out of *Acan* in visual cortex of adult mice disintegrates PNNs. **a:** Experimental time line and schematic illustration indicating injection of AAV9.CreGFP (AAV9.Cre) in V1 of Acan-loxP^{+/+} mice. **b** and **c:** WFA labeled PNNs gradually disappear over time within the

AAV9.Cre treated area. Sections were co-stained for GFP to identify transfected neurons. Three weeks after injection the transfected neurons produced the GFP-Cre fusion protein. After 8 weeks all PNNs in the injected area in V1 were abolished. Fluorescence intensity measurements of WFA staining were significantly lower in the AAV9.Cre treated area compared to the corresponding area in the contralateral untreated hemisphere, $p=0.0006$ (paired t-test, $n=6$ mice). Measurements were performed across all cortical layers and averaged from 3 sections for each animal. **d** and **e**: Representative confocal images from AAV9.Cre treated area within V1 and the corresponding area in the contralateral untreated hemisphere from the same section. Local knock-out of *Acan* in V1 removed staining for aggrecan as well as Crtl-1, tenascin-R, versican and neurocan.

Fig. 4: Local removal of *Acan* in V1 reactivates juvenile ocular dominance plasticity.

a: Injection of the retrograde tracer Cholera toxin subunit B (CtxB) conjugated to different fluorphores, at two closely aligned sites in V1 of non-targeted *Acan-loxP^{+/+}* mice. Representative wide-field image from V1 (upper) and confocal images from the dorsal part of the lateral geniculate nucleus (dLGN) of the thalamus. Labeled projections stem from adjacent patches of neurons in dLGN, indicating a normal connectivity pattern with retinotopic organization. Sections were counter-stained with DAPI to distinguish brain areas, and data was reproduced in two mice. **b:** Experimental time line for optical imaging of intrinsic signals before and after monocular deprivation (MD) of adult mice. **c:** Ocular dominance index (ODI) calculated for responses to stimulating the ipsi –and contralateral eye separately, before and after four days of MD. Positive ODI indicates contralateral bias while negative ODI indicates ipsilateral bias. Four days of MD did not affect ocular dominance in non-injected *Acan-loxP^{+/+}* mice ($p=0.21$, paired t-test, $n=4$ mice) or in heterozygous AAV9.Cre injected *Acan-loxP^{+/-}* mice ($p=0.32$, paired t-test, $n=3$ mice). In AAV9.Cre injected *Acan-loxP^{+/+}* mice, MD caused a significant shift in activation towards the open eye ($p=0.003$, paired t-test, $n=7$ mice). **d:** Stimulus evoked responses of intrinsic signals through the open or closed eye before and after four days of MD. The MD in AAV9.Cre injected *Acan-loxP^{+/+}* caused both increased responses to ipsilateral stimulation ($p=0.02$, paired t-test, $n=7$ mice) and reduced responses to contralateral stimulation ($p=0.009$, paired-test, $n=7$ mice), while no effect was observed in controls. *Acan-loxP^{+/+}*, deprived eye responses: $p=0.73$ (Wilcoxon signed rank test), open eye responses: $p=0.48$ (paired t-test), *Acan-loxP^{+/-}* AAV9.Cre injected, deprived eye responses: $p=0.46$

636 (paired t-test), open eye responses: $p=0.70$ (paired t-test). Open circles and grey lines indicates individual
637 animals, solid circles and thick lines indicate population mean \pm standard deviation.

638

639

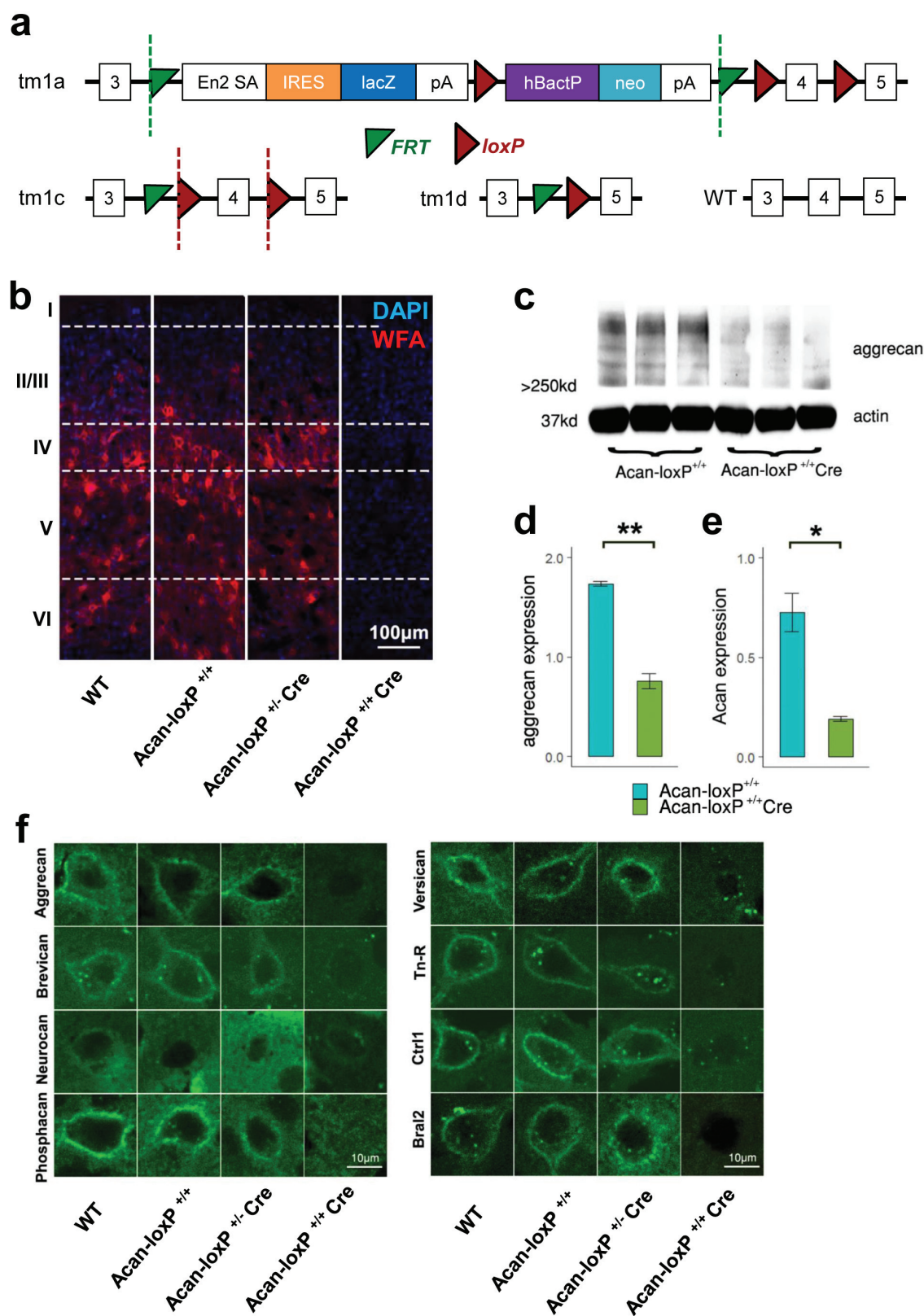
640 **Fig. 5: Targeting of *Acan* enhances object recognition memory.**

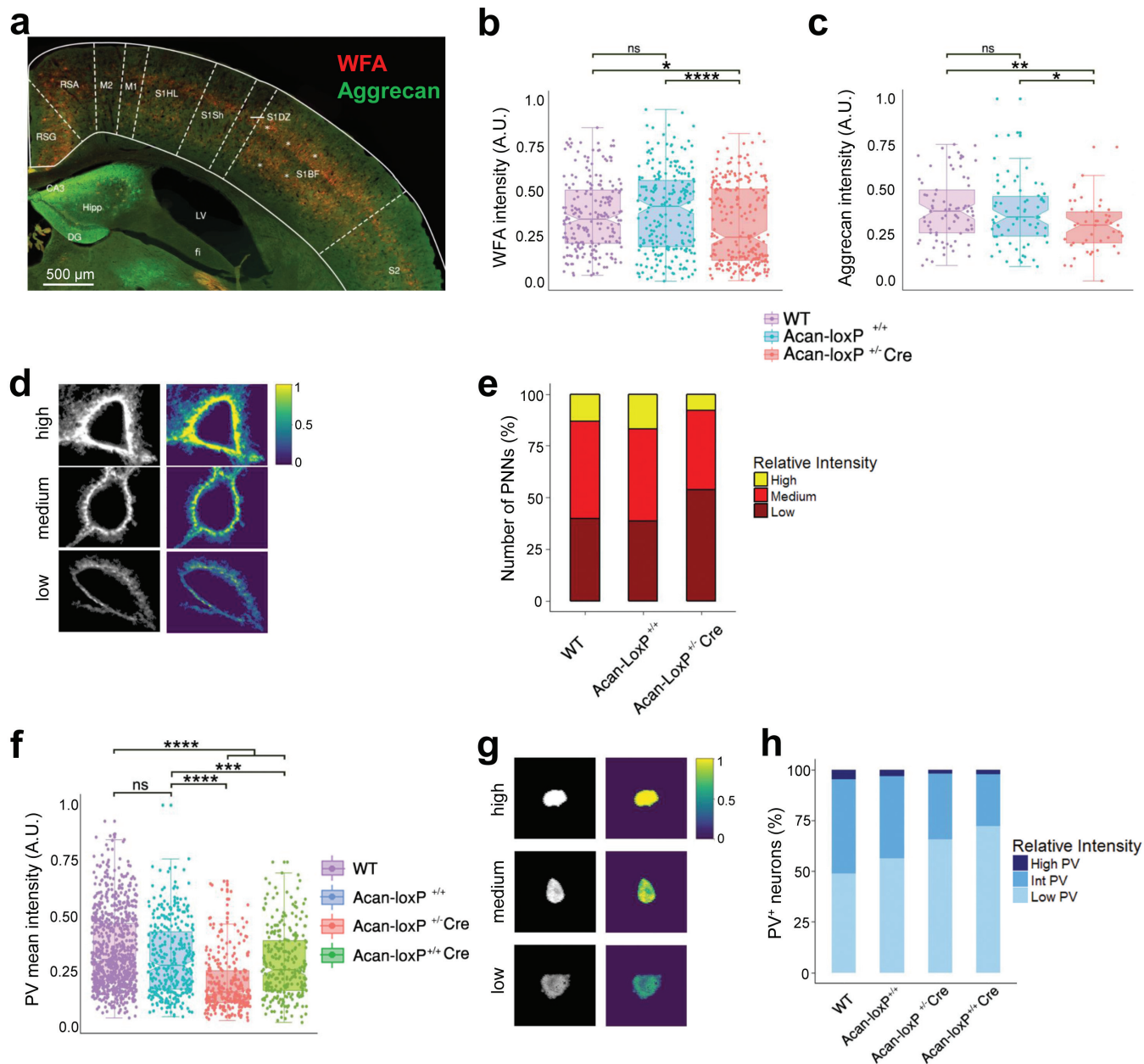
641 **a:** Diagram of the experimental paradigm. **b:** Mean sample times of WT, *Acan-loxP^{+/+}*, *Acan-loxP^{+/-}*Cre
642 and *Acan-loxP^{+/+}*Cre for 3 hour and 24 hour sample phases during spontaneous object recognition testing.
643 All animals participated well in the test with the average exploration time about 40 seconds. **c:** Mean
644 object recognition scores following 3 hour and 24 hour delays. A significant decrease in object
645 recognition ability was detected in the WT, *Acan-loxP^{+/+}* and *Acan-loxP^{+/-}*Cre groups following a 24
646 delay between sample and choice phases while *Acan-loxP^{+/+}*Cre did not. ** = $p < 0.01$, * = $p < 0.05$, ns =
647 not significant.

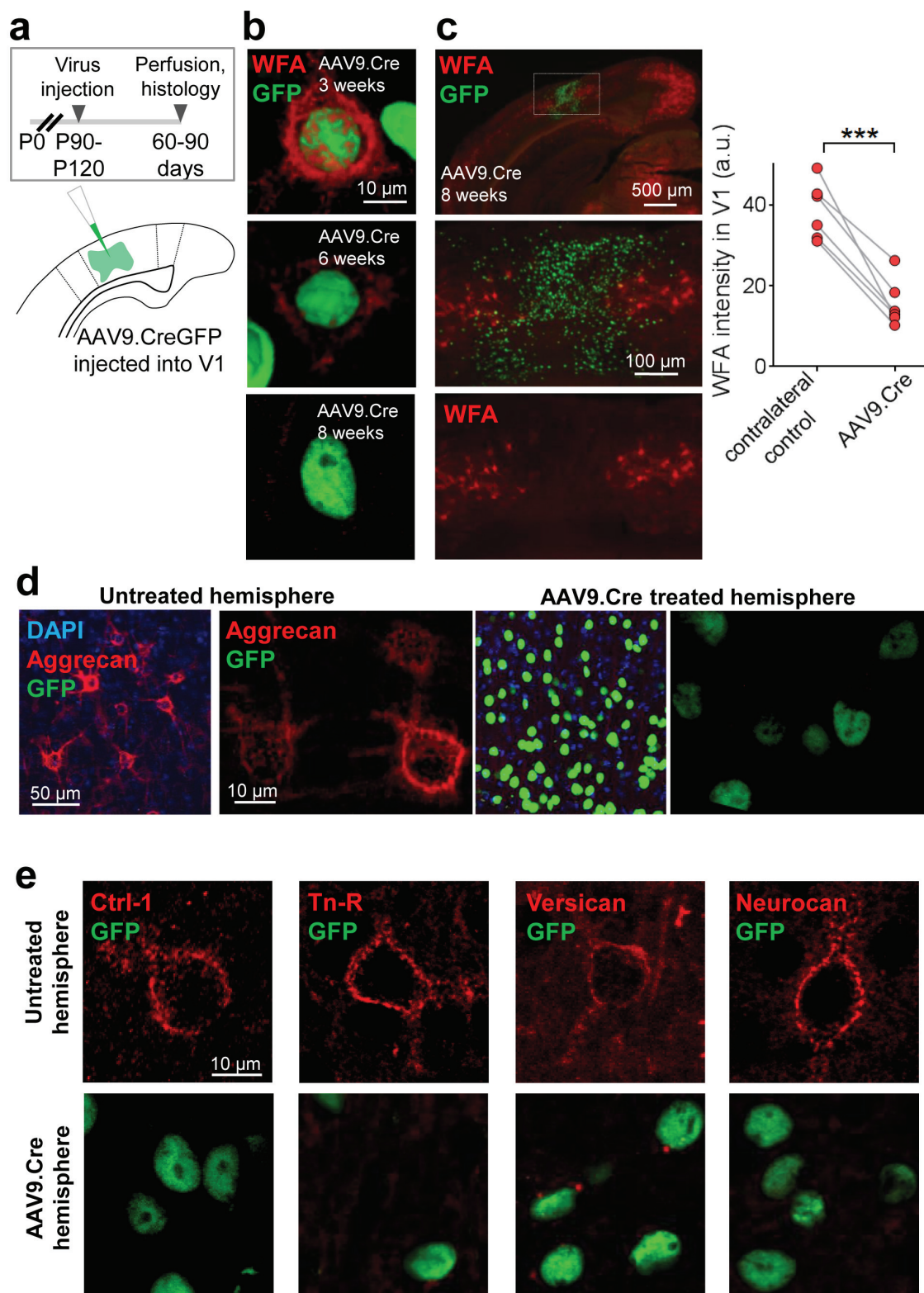
648

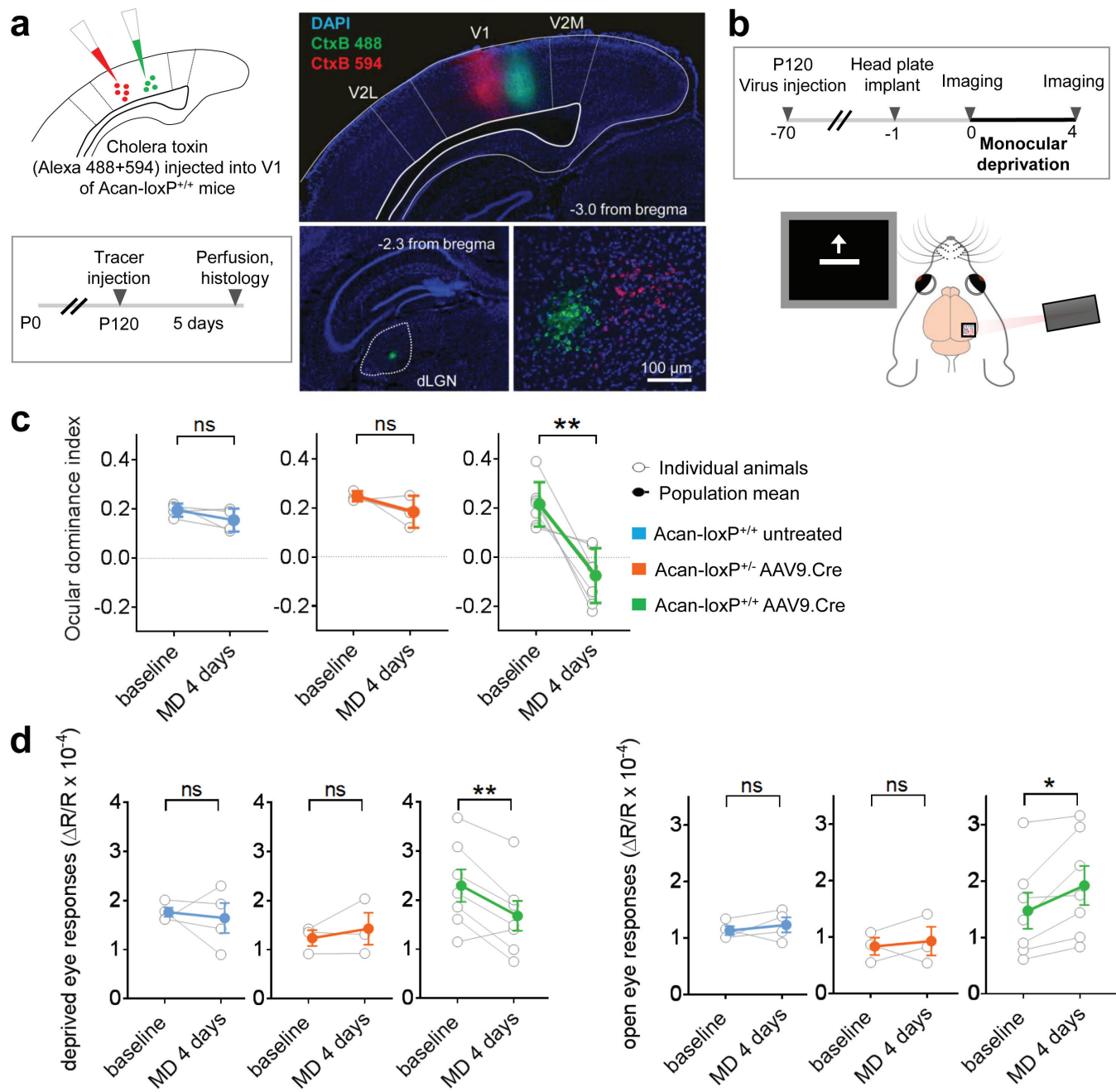
649

650

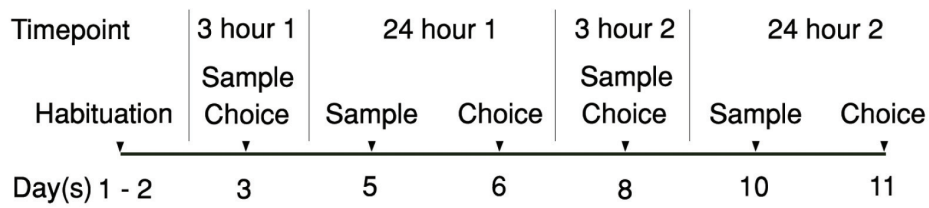




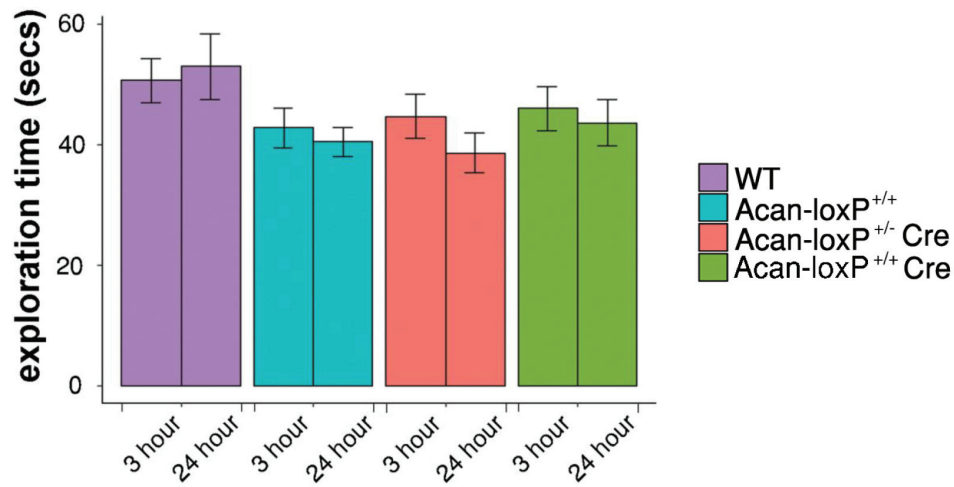




a



b



c

